Paul Day
Department of Mechanical Engineering,
Stanford University,
Stanford, CA 94305;
and Los Alamos National Labs,
Los Alamos, NM 87544
e-mail: pday@stanford.edu

Eric V. Eason
Department of Applied Physics,
Stanford University,
Stanford, CA 94305
e-mail: easone@stanford.edu

Noe Esparza
e-mail: noe.esparza@stanford.edu

David Christensen
e-mail: davidc10@stanford.edu

Mark Cutkosky
e-mail: cutkosky@stanford.edu

Department of Mechanical Engineering,
Stanford University,
Stanford, CA 94305

Micro-Wedge Machining for the Manufacture of Directional Dry Adhesives

Directional dry adhesives are inspired by animals such as geckos and are a particularly useful technology for climbing applications. Previously, they have generally been manufactured using photolithographic processes. This paper presents a micro-machining process that involves making cuts in a soft material using a sharp, lubricated tool to create closely spaced negative cavities of a desired shape. The machined material becomes a mold into which an elastomer is cast to create the directional adhesive. The trajectory of the tool can be varied to avoid plastic flow of the mold material that may adversely affect adjacent cavities. The relationship between tool trajectory and resulting cavity shape is established through modeling and process characterization experiments. This micro-machining process is much less expensive than previous photolithographic processes used to create similar features and allows greater flexibility with respect to the micro-scale feature geometry, mold size, and mold material. The micro-machining process produces controllable, directional adhesives, where the normal adhesion increases with shear loading in a preferred direction. This is verified by multi-axis force testing on a flat glass substrate. Upon application of a post-treatment to decrease the roughness of the engaging surfaces of the features after casting, the adhesives significantly outperform comparable directional adhesives made from a photolithographic mold.

Keywords: directional, adhesion, gecko, manufacturing, micro-machining

1 Introduction

Impressive advancements have been made in the field of gecko-inspired fibrillar dry adhesives. Fearing [1] maintains a bibliography of the manufacturing methods for these adhesives, which include a large range of manufacturing processes. However, the use of such adhesives in applications such as climbing has been much more limited, with just a few examples reported [2–8]. It has generally been found that the adhesion levels generated in real-world climbing applications are significantly lower than those obtained using small samples in bench-top experiments.

One reason for this disparity is that, in addition to conforming to surfaces and generating useful levels of adhesion, the adhesives have additional requirements when used for climbing. The first of these requirements is controllability, i.e., the adhesives should not be sticky in the default state and adhere only when it is desirable. In any other case, energy will be wasted as it is expended in attaching and detaching the adhesive for each step. Controllability can be achieved by using switchable structures [9, 10] or by creating directional adhesive features whose adhesion generation is a function of applied shear load [11–24].

The second requirement is durability. The adhesives must undergo thousands of attach/detach cycles without significant loss of adhesive properties and, ideally, should resist fouling and be easy to clean. Durability is also correlated with controllability: gentle attach/detach cycles reduce mechanical wear and promote long life [18].

Among the adhesives that have been applied to climbing robots, micro-wedges [18] are simple and durable structures that have enabled kilogram-scale robots to climb on glass, plastic, wood paneling, painted metal, and similar surfaces. In particular, the 0.8 kg StickybotIII robot climbs using approximately 7 cm^2 of adhesive per foot, and the 4 kg RiSE robot climbs using approximately 20 cm^2 per foot (both robots have four feet and lift two at a time) [25]. Micro-wedges present a very small real area of contact with a surface and generate negligible adhesion when they are unloaded, as in Fig. 1a. However, when loaded in a preferred shear direction, as in Fig. 1b, they bend, creating a larger contact area and generating adhesion that is proportional to the shear load. The micro-wedges' asymmetric taper ensures that the radius of curvature of the surface at the proximal edge of the contact patch increases with increasing shear load, allowing the tapered features to outperform features of constant cross-section at high shear loads [26]. Furthermore, they may be easily cleaned using a piece of sticky tape.

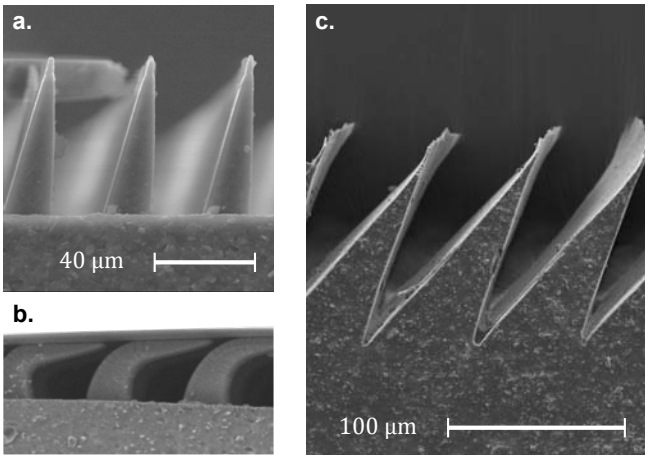

Fig. 1 SEM micrographs of PDMS directional adhesive features: (*a*) unloaded micro-wedges from a photolithographic mold, (*b*) micro-wedges under shear loading, and (*c*) micro-wedges from a micro-machined mold.

In previous work, micro-wedges were manufactured by casting a polydimethylsiloxane (PDMS) silicone elastomer into molds cre-

ated through a photolithographic process in which SU-8 photoresist (MicroChem Corp.) was subjected to two exposures, one angled, one vertical, through contact masks [18]. The necessity of a thick photo-resist layer combined with the requirement for high precision alignment of exposures resulted in a time consuming, expensive mold fabrication process with relatively low yield.

As an alternative, a mold can be created with a micro-machining process that involves making a pattern of cavities in a mold using a narrow cutting tool. Machining processes have been used previously to create stamps for soft lithography [27] and synthetic adhesive structures [11, 28] using nano-indenters and AFM tips, but neither fabrication nor testing of macroscopic adhesive arrays (~ 1 cm^2) has been demonstrated and the aspect ratio of the resulting features has been low.

This paper introduces a micro-machining process that is a hybrid of orthogonal machining and wedge indenting. A sharp wedge-shaped tool is moved along an oblique trajectory into a soft mold surface, producing a wedge-shaped cavity of depth on the order of 100 µm. By controlling the tool geometry and trajectory and repeating this operation in a pattern across the mold surface, it is possible to obtain a dense packing of sharp, wedge-shaped cavities. Casting PDMS into these cavities produces micro-wedge features as seen in Fig. 1c. In comparison to photolithography, the method presented here is cheaper, faster, and affords greater freedom to control the cavity geometry, which governs adhesive performance.

The main motivation of this research is the need for a practical adhesive for climbing. The new micro-machined micro-wedges, upon application of a simple post-treatment process, perform significantly better than photolithographic micro-wedges in adhesive tests. The improvement is chiefly a result of having greater freedom to control the wedge taper and angle of inclination. Arrays of the new wedges have been produced and tested, with maximum normal adhesion of 38 ± 2 kPa attained at a shear stress of 49 ± 1 kPa for an array of area 1.21 cm^2. In addition, the micro-machined wedges retain the controllability and durability of photolithographic wedges.

In Sec. 2, a simple model of the micro-machining process is introduced to explore the relationships among tool geometry, tool trajectory, wedge geometry, and the ability to achieve a dense feature spacing. Section 3 gives details of the adhesive fabrication process. In Sec. 4, the model is compared to experimental cutting forces, process characterization results are presented, and the adhesive performance of the new micro-machined adhesives is measured and compared to the previous generation of photolithographic adhesives. These results are discussed in Sec. 5. Section 6 presents conclusions and possible extensions.

2 Modeling

In order to better understand the mechanics involved, a micro-machining process may be described using numerical finite-element modeling or semi-analytic theoretical models. Theoretical models are mostly applied to ideal rigid-plastic materials and are not as likely to accurately predict the forces and deformations. Conversely, state of the art numerical models can account for realistic material behavior and friction effects. However, the material properties and tribological behavior of the wax mold material used here have not been sufficiently well characterized to justify a numerical model. Moreover, it is not required to produce a numerical prediction of the cutting forces in terms of the cutting parameters (e.g. cutting depth, speed, friction, tool angle, or tip radius) as the forces are, in any case, quite low.

Instead, it is useful to understand how the cutting parameters and tool geometry affect the deformation behavior. In particular, it is desirable to produce a tightly packed array of cavities in order to obtain a high density of adhesive features. Accordingly, an important question is whether displaced material is moved mainly in the forward direction (towards the unmachined part of the mold) or the rearward (tending to close up the previously made cavity). Semi-analytic theoretical models can provide this insight without recourse to running numerous simulations, which may be poorly convergent or sensitive to boundary conditions and may require frequent remeshing due to the large deformations involved.

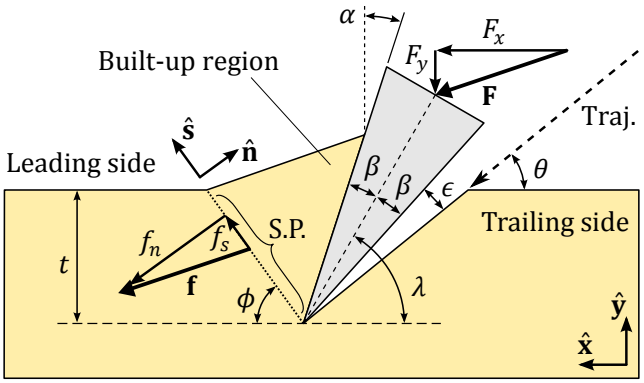

Fig. 2 A diagram illustrating the geometry and the parameters of the micro-machining process for a single cavity. "Traj." is the tool trajectory; "S.P." is the shear plane.

2.1 Assumptions. If the cutting depth t and the tool cross-section are constant along the width of the cavity (into or out of the page in Fig. 2), and if t is much smaller than the width of the cavity, then the stressed material is confined to a long, narrow prismatic region. In the experiments described here, $t \leq 100$ µm and the cavity width is greater than 10 mm, so it is reasonable to assume that the material is in a state of plane strain.

The process bears resemblance to two classical problems from plane-strain plasticity theory: oblique wedge indenting [29, 30], in which a rigid wedge-shaped tool penetrates the work surface, and orthogonal machining [31–33], in which the tool removes a thin strip of material by moving parallel to the work surface. As noted by Johnson *et al.* [34], some of the proposed solutions for wedge indenting and orthogonal machining show similarities. The process under present consideration is a generalization of the two processes: the tool is wedge-shaped with internal angle 2β, the centerline of the tool is set at an angle λ with respect to the work surface, and the direction of motion of the tool is neither parallel to the centerline (as in wedge indenting) nor to the work surface (as in orthogonal machining), but instead is set at an intermediate angle $0 < \theta < \lambda$, as shown in Fig. 2.

To model this process analytically, it is assumed that the work material is perfectly rigid-plastic. While most plasticity studies have been concerned with the plastic behavior of metals, wax has also been used as a work material [35, 36], and waxes can be closer to rigid-plastic than metals. The wax used here has been found through axial compression testing to have a low shear yield strength (approximately 2 MPa) and little work hardening; however, it does exhibit some elastic recovery, which can affect the forces and cavity geometry during micro-machining.

Given these assumptions, it is feasible to adapt an existing semi-analytic model to the present situation to obtain an estimate of the flow of material on both sides of the tool and the expected buildup region adjacent to the cavity. Consider the model proposed by Meguid and Collins [37], which is an extension of Hill's wedge indenting solution [30] to the case where a rigid, frictionless wedge enters the material obliquely. Meguid and Collins assume that the

wedge's direction of motion is along its centerline, but their model can be easily modified to allow yawed motion (not parallel to the centerline) by considering the leading and trailing sides of the tool independently as in an earlier model by Hill and Lee [38].

2.2 Trajectory Angle. For a perfect rigid-plastic material, the interior shape of the cavity will be identical to the swept volume of the tool as it moves along its trajectory, which means that any trajectory angle θ can be chosen from the range $\lambda - \beta < \theta < \lambda + \beta$ without affecting the shape of the cavity. However, the extent of plastic deformation and the amount of buildup occurring on the leading and trailing faces of the tool will vary with θ. If material is displaced on both sides of the tool, and the mold cavities are spaced closely, this flow will result in partial collapse of the previously formed cavity.

In order to minimize this effect, the trajectory angle may instead be chosen to lie outside this range: $\theta = \lambda - \beta - \epsilon$, where $\epsilon > 0$ is a relief angle. This increases the angular width of the cavities by the angle ϵ. A depiction of this geometry can be seen in Fig. 2. The benefit of the relief angle is that the trailing side of the tool should no longer make contact with the wall of the cavity. As a result, assuming that the tip of the tool is sufficiently sharp [36,39], the zone of plastic deformation is limited to the leading side of the tool only, and material on the trailing side remains rigid throughout the process, theoretically preventing partial collapse of the previous cavity.

2.3 Plastic Region. The Meguid-Collins model predicts two possibilities for the plastic deformation on the leading side of the tool. In the first case, the plastic region covers the entire area of displaced material, and it is possible to construct a slip-line field throughout this region, similar to the Hill model of wedge indenting [30]. In the second case, the plastic region is restricted to a single shear plane, and elsewhere the material is rigid, in a similar manner to the Merchant model of orthogonal machining [32, 33]. This second case occurs if the trajectory angle is lower than a critical value:

$$2\tan\theta < [1 + \tan(\alpha + \theta)]^2 \tag{1}$$

However, this equation is always satisfied if the rake angle α is positive, as in the present case. Therefore, the model predicts that a single shear plane solution is appropriate on the leading face of the tool. The model also provides a prediction of the shear plane angle ϕ based on an energy-minimization argument similar to the one proposed by Ernst and Merchant [31], but since the model does not include friction this prediction is not expected to be accurate. Furthermore, there is doubt about the theoretical and experimental validity of this argument [40–42].

2.4 Cutting Forces. Despite the lack of a trustworthy prediction of the shear plane angle ϕ, the model can be used to make a testable prediction about the cutting forces if ϕ can be measured experimentally. Let the net force applied by the machine to the tool be denoted by

$$\mathbf{F} = F_x\hat{\mathbf{x}} + F_y\hat{\mathbf{y}} \tag{2}$$

and let the total force on the shear plane be denoted by

$$\mathbf{f} = f_s\hat{\mathbf{s}} + f_n\hat{\mathbf{n}} \tag{3}$$

as depicted in Fig. 2. In accordance with the model, it is assumed that the displaced material is limited to a triangular built-up region also shown in Fig. 2. As long as there is no contact on the trailing side of the tool, these forces are equal: $\mathbf{F} = \mathbf{f}$, and therefore:

$$f_s = F_x(\hat{\mathbf{x}} \cdot \hat{\mathbf{s}}) + F_y(\hat{\mathbf{y}} \cdot \hat{\mathbf{s}}) = F_x\cos\phi + F_y\sin\phi \tag{4}$$

This relationship does not require any assumptions about the shear plane angle ϕ or the friction at the leading side of the tool. Finally, according to the theory of perfect rigid-plastic materials in plane strain [40], the shear stress along the shear plane is constant and equal to the shear yield stress k:

$$f_s/A = k \tag{5}$$

where A is the area of the shear plane.

Although the semi-analytic model cannot be expected to produce a complete prediction of the cutting forces with high accuracy, it produces a useful prediction about the deformation mode of the material (the existence of a shear plane), and it is also useful for understanding relationships among λ, β, θ, and ϕ. This leads to the expectation that most of the displaced material will be pushed forward if the trajectory angle, θ, is sufficiently small compared to the angle of the trailing face of the tool, $\lambda - \beta$. In this situation, the model does produce a testable prediction about the cutting forces (Eqs. 4 and 5).

3 Fabrication

3.1 Materials. The mold fabrication method relies on a few key components to be effective. Most important is the wedge-shaped tool, whose shape strongly influences the shape of the resulting mold cavities. The tool used here is a PTFE-coated steel disposable microtome blade (Delaware Diamond Knives D554X). This tool has a fine surface finish, with blade roughness on length scales $\ll 1$ μm, an internal angle of $2\beta \approx 24°$, and an edge radius of less than 0.9 μm (see Sec. 4.1).

The material used for the mold must also be selected for desirable properties. An ideal material for machining would have a homogeneous composition, a relatively low yield strength, and perfect rigid-plastic behavior to minimize elastic recovery of the machined region. As noted by Hirst and Howse [43], rigid-plastic behavior is most likely to occur in indenting processes if the included angle of the tool is acute and the ratio of Young's modulus to yield stress E/Y is large.

In the present case, a soft, rolled sheet wax (Kindt-Collins Master Regular Sheet Wax) is used, having a ratio of Young's modulus to yield stress of approximately $E/Y \approx 110$–160. For this value of E/Y with a tool angle of 24°, according to the results presented by Hirst and Howse, the deformation behavior is not dominated by elastic effects and rigid-plastic behavior may be possible.

Adhesive wear at the tool-mold interface is undesirable and could lead to a poor surface finish. However, this is mitigated by lubricating the interface. In addition a post-treating process has been devised to refinish the surfaces entirely (Sec. 3.4). For these reasons the tribological properties of the mold material are not a major concern for material selection.

3.2 Micro-Machining Method. This micro-machining process may be performed on a standard CNC milling machine or other machine with positioning control in at least two axes and sufficient accuracy. Adhesives have been produced using a tabletop CNC milling machine with 1 μm accuracy (Levil WL400), a larger

CNC milling machine with 2.5 μm accuracy (Haas VF-0E), and a motorized stage with an estimated accuracy of 10 μm (Velmex MAXY4009C-S4 and Newport GTS30V). For micro-machining, however, the repeatability over small areas is of greater relevance than the accuracy over the entire workspace of the machine.

Ultimately, the dimensions of an adhesive patch are constrained only by the width of the microtome blade and the length of the workspace of the machine. With the equipment described above, it is possible to make a single uninterrupted patch of adhesive as large as 76 mm wide by 762 mm long.

First, the wax is melted and cast into a block to improve the consistency of its plastic behavior and to obtain a desirable form factor for fixturing, and then it is cooled to room temperature. The mold surface is milled and planed to ensure it is flat and parallel to the machine ways. Next, the surface is cleaned and the micro-machining tool is mounted to the machine head. The blade is fixed so that its centerline is tilted by a constant angle of $\lambda = 60°$ with respect to the horizontal surface of the wax (see Fig. 2). The tip of the blade is then aligned to the wax surface.

3.2.1 Tool Trajectory. The tool is moved by the machine along a specified 2-D trajectory into the wax until its tip reaches a desired depth t in the negative y-direction (see Fig. 2). At this point the tool is retracted above the surface and then advanced a set distance in the positive x-direction to create a space between cuts. The cycle then repeats.

The tool trajectory may be chosen from a large space of possible paths. Varying the trajectory provides freedom to control the completed cavity shape and the plastic flow of the mold material. Attempts to characterize the indenting process as a function of the trajectory are described in Sec. 4.3.

3.2.2 Lubrication. Without lubrication, adhesive wear occurs between the tool and the mold material. SEM examination of the micro-wedges cast from these molds indicates significant surface roughness on critical areas such as the engaging faces that will ultimately generate adhesion (see Fig. 3a). To address this issue, a lubricant has been added to the process to inhibit material transfer from the wax mold to the tool. Several fluids were tested, including various mixtures of water and surfactants in the form of liquid dish soaps. The resulting surfaces were characterized using SEM 3D stereo microscopy, as described in Sec. 4.4. The lowest roughness was obtained with a 10:2 concentration of Ajax liquid dish soap (Colgate-Palmolive) to water. This improvement in surface finish can be seen in Fig. 3b.

3.3 Casting. The completed mold is cleaned with solvents and water to remove all traces of lubricant. A PDMS silicone elastomer (Dow Corning Sylgard 170) is vacuum de-gassed and poured into the mold. For samples for adhesion force testing, a 300 μm thick backing layer of PDMS is desired. This can be achieved by spinning the mold at 160 RPM for 30 seconds, or alternatively a two-part mold may be created by placing a flat sheet of glass upon 300 μm supports which rest on the wax mold surface. For climbing applications [7], the sheet of glass may be replaced by a rigid tile made of glass fiber or aluminum. The tile is treated with a primer (Dow Corning PR-1200), which allows the PDMS to bond directly to the tile. In any case, the casting is then allowed to cure at room temperature for 24 hours (heat acceleration is not suitable due to thermal expansion of the wax). Once removed from the mold, the elastomeric adhesive is ready for use. The mold may become damaged as the castings are de-molded, in which case the mold may be resurfaced and micromachined again before its next use (see discussion in Sec. 5).

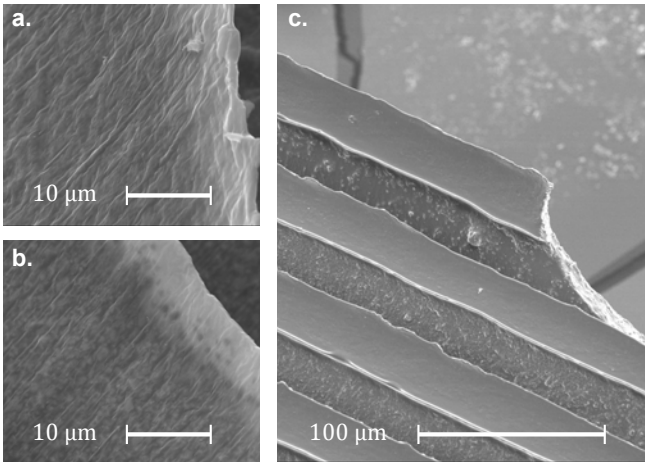

Fig. 3 Surface comparison of PDMS micro-wedges cast from micro-machined wax molds, using (*a*) no lubricant, (*b*) liquid soap lubricant, and (*c*) liquid soap lubricant and "inking" post-treatment. A broken wedge, illustrating the wedges' tapered profile, can be seen on the right.

3.4 Post-treatment. While the addition of lubrication to the micro-machining process improves the surface finish of the molds and molded wedges, there is still remaining roughness that affects the performance of the adhesives by reducing the real area of contact between the adhesive and the substrate. In order to further reduce this roughness, a post-treatment is employed after casting. This treatment adds a thin, smooth secondary layer of PDMS to the engaging faces of the wedges. The treatment proceeds as follows (see Fig. 4):

1. Uncured PDMS is diluted to a concentration of 10% toluene by volume. The diluted mixture is then poured onto a four-inch quartz wafer and spun at 8000 RPM for 60 seconds to obtain a uniform thin layer 3–5 μm thick.
2. One half of the wafer is cleaned using isopropyl alcohol, and the wafer and a cast adhesive sample are secured to a three axis motorized positioning stage (described in Sec. 4.5). The adhesive sample is aligned using the positioning stage's two-axis goniometer.
3. The sample is brought into contact with the PDMS-coated half of the wafer. After applying a normal load so that the wedges are in contact with the wafer over approximately one third of their length, the adhesive is taken out of contact, leaving a thin, wet layer of PDMS on the tips of the wedges.
4. After this "inking" procedure, the adhesive is loaded against the cleaned half of the wafer and held there in order to flatten this thin, wet layer as it cures.
5. The cured thin layer binds strongly to the previously cured wedges. The post-treatment results in smooth patches of PDMS on the engaging faces of the wedges (see Fig. 3c).

Although the thin layer of PDMS deposited on the tips of the wedges is smooth, the surface roughness of the wedges in the subjacent region near the bottom of the wedges appears to be adversely affected by post-treatment (this roughness is visible in Fig. 3c). However, this region does not contact the substrate unless the adhesive is subjected to extreme loads.

For a climbing adhesive which has been cast directly to a rigid tile, the post-treatment may be done without the motorized positioning stage, by simply using an appropriately sized weight. In this variation of the process, the wafer is placed on a flat surface, the adhesive is placed on the wafer (with the back of the tile facing up),

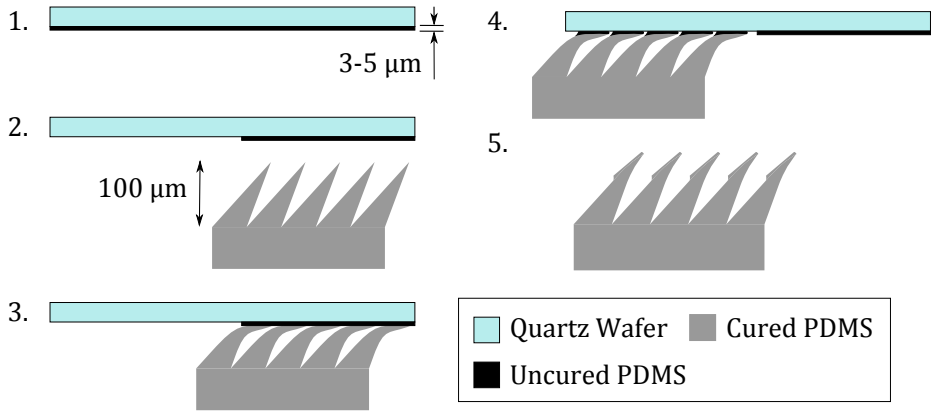

Fig. 4 Diagram illustrating the steps of the post-treatment process (see text for details)

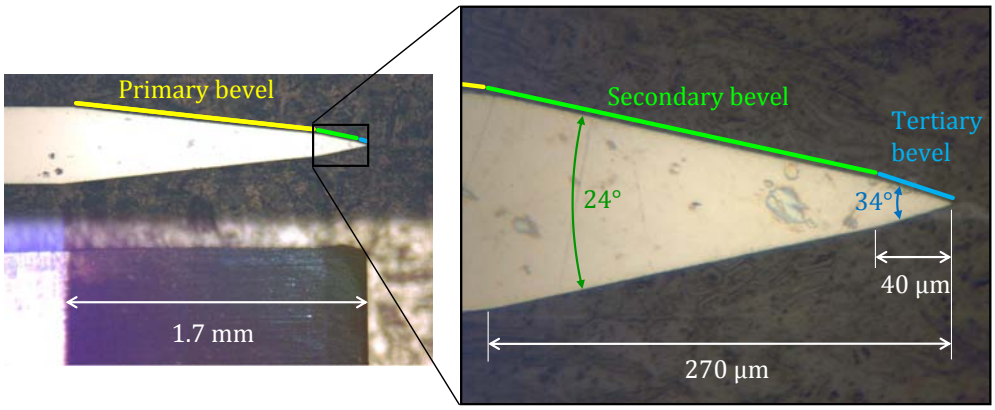

Fig. 5 Cross-section of microtome blade used in the micro-machining process, showing its three different beveled sections

and the weight is placed on the tile. This passive alignment technique is more effective than using a rigid positioning stage for large adhesive tiles, because it becomes increasingly difficult to actively align the surfaces as their size increases. Using weights instead of a positioning stage, angular alignment within 0.03° has been achieved (less than 20 μm of height misalignment over a 44 mm length of adhesive). The best post-treatment results have been obtained using weights such that the average pressure is approximately 7–8 kPa, but this depends on the shape and stiffness of the wedges.

4 Results

Experiments were performed to test the semi-analytic model introduced in Sec. 2, to empirically characterize the micro-machining process, to characterize the surface roughness of the micro-machined micro-wedges, and to measure the adhesive performance of macroscopic arrays of wedges. These experiments and their results are presented in Secs. 4.2, 4.3, 4.4, and 4.5. However, it is first necessary to look more closely at the geometry of the microtome blades used here as micro-machining tools.

4.1 Tool Geometry. As seen in Fig. 5, the blades are not simply a triangular wedge. Instead, the manufacturer has sharpened them to a profile with three different beveled sections. The primary bevel begins approximately 1.7 mm from the tip and has an angle of 12° (this section is above the wax mold at all times). The secondary bevel begins 270 μm from the tip and has an angle of 24°, and the tertiary bevel extends over the final 40 μm of the blade's length and is 34° wide. The tip is too small to be seen at this magnification, but an upper limit radius of 0.9 μm may be established.

In the described machining geometry, the border between the secondary and tertiary bevels is below the surface of the wax whenever the blade is inserted more than 40 μm deep. However, the mold cavities created by the micro-machining process (with a nominal depth of 100 μm) show little evidence of this border, and the terminal angle of the PDMS wedges is considerably narrower than the tertiary blade bevel. This implies that there is significant elastic behavior occurring in the mold material, as the tips of the mold cavities are narrowing by several degrees when the blade is retracted. This effect is observed for single cavities as well as arrays of cavities.

4.2 Cutting Force Tests. To test the predictions of the semi-analytic model, the cutting forces during micro-machining were measured. A wax specimen of width 1 cm was attached to a six-axis force/torque sensor (ATI Gamma SI-32-2.5) which was mounted in a CNC milling machine, and a variety of micro-machining trajectories were used to create cavities in the wax. The trajectories were linear and differed by trajectory angle, ranging from $\theta = 36°$ to 60°, and maximum depth, ranging from $t = 20$ μm to 100 μm. The blade centerline angle was $\lambda = 60°$ in all cases, an angle found empirically to produce adhesive features with the desired directional behavior. In this experiment, the cavities were spaced far apart (0.5 mm tip-to-tip) so that the interaction between them was negligible. The blade was wider than the wax specimen so that its corners were not in contact.

The resulting force data were analyzed to find the cutting force $\mathbf{F}$ corresponding to the endpoint of each trajectory, the point in time when the tool was at its maximum cutting depth t for each cavity.

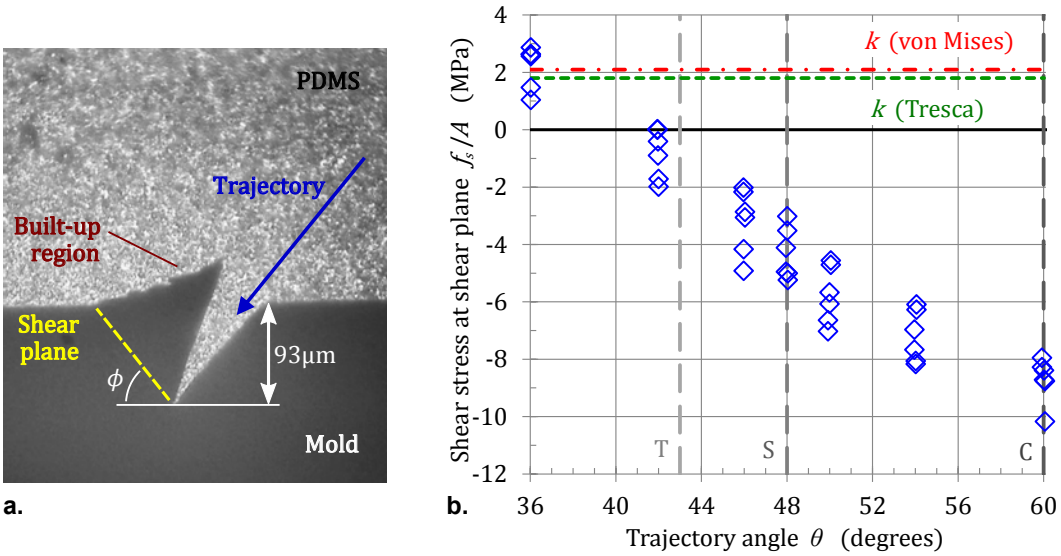

Fig. 6 (*a*) Micrograph of a single mold cavity created in cutting force tests ($\theta = 50°$, $t = 100$ μm) showing triangular built-up region. (*b*) Measured shear stress at the shear plane f_s/A versus θ, with values of shear yield stress k for comparison. T, S, and C correspond to trajectories parallel to the tertiary bevel, secondary bevel, and centerline of the tool. The estimated measurement uncertainties of θ and f_s/A are 0.6° and 0.8 MPa.

The final cavity shape, preserved by casting PDMS into the specimen, serves as a record of the shape of the cavity at that same point in time. As shown in Fig. 6a, these castings clearly show the triangular shape of the built-up material adjacent to the leading side of the tool (consistent with the model). By constructing a line from the tip of the cavity to the front edge of the built-up region, and taking into account the width of the wax specimen, it is possible to measure the area of the shear plane A and the shear plane angle ϕ (Fig. 6). The ϕ measurement has an estimated uncertainty of 4°.

For each cavity, the value of $\mathbf{F}$ was projected onto the shear plane using Eq. 4 to produce an estimate of the shear stress f_s/A. This equation is only accurate if there is no contact between the trailing side of the tool and the wax. If there is such contact, the measured cutting force $\mathbf{F}$ will be the sum of forces at the leading and trailing tool faces, which cannot be separated using external measurements.

The measured values of f_s/A versus θ are plotted in Fig. 6b. In addition, the shear yield stress of the wax k was calculated from the compressive yield stress (which was determined through axial compression testing) by using either the Tresca or von Mises shear yield criterion. The uncertainty in f_s/A is estimated to be 0.8 MPa based on the propagation of measurement uncertainties in ϕ, A, and $\mathbf{F}$.

Even though the cutting depth varied from $t = 20$ μm to 100 μm for each trajectory, causing some variance in the data, the trend is the same for all values of t. For trajectories near $\theta = \lambda = 60°$, there is substantial disagreement between the measurements of f_s/A and the value of k, using either the Tresca or von Mises yield criteria. The direction of the cutting force $\mathbf{F}$ is nearly *antiparallel* to the shear plane, causing f_s to be negative instead of positive. This may be due to contact forces on the trailing side of the tool because, for trajectories $\theta > 43°$, it is expected that the secondary or tertiary bevels will contact the wax on the trailing side, due to the blade geometry discussed in Sec. 4.1.

For trajectories $\theta < 43°$, it is expected that there is no contact on the trailing side of the tool, and therefore the measured value of f_s/A should be equal to k in accordance with Eq. 5. Indeed, the data for the shallowest trajectory, $\theta = 36°$, are in agreement with Eq. 5. However, the data for $\theta = 42°$ are not. This disagreement cannot be explained completely by the geometry of the blade. In this case, it is likely that contact is occuring on the trailing side of the blade. This may be due to elastic recovery of the wax (which was assumed negligible in the model) or it may be that the tribological interaction between the tool, lubricant, and mold surface is more complicated than can be described in this simple model.

In summary, the evidence appears to invalidate the assumption that the material on the trailing side of the tool is rigid, for the majority of the micro-machining trajectories tested. Theoretical modeling has provided useful qualitative insight into the micro-machining process, but the models considered here are unable to explain the actual cutting forces, and they cannot necessarily be used to predict the deformation of the mold material in a process that involves multiple cavities being formed in series. These realizations prompted an empirical investigation of the micro-machining process.

4.3 Empirical Micro-Machining Characterization. Predicting the cutting force is not strictly necessary to produce a useful adhesive mold insofar as the forces are small enough not to damage or significantly deflect the micro-machining tool. However, it is important to ascertain the effect of the micro-machining trajectory on the shape of the mold cavities. To accomplish this, a characterization experiment was performed in which the trajectory angle was varied (again from $\theta = 36°$ to 60°) while the nominal depth and tip-to-tip spacing of the cavities were kept constant at 100 μm and 60 μm respectively. At this depth and spacing, the cavity shapes were expected to be significantly influenced by neighboring cavities, so a series of ten cavities was made for each trajectory.

PDMS was cast into the mold cavities and the resulting adhesive samples were cut in cross-section and measured with a microscope, as shown in Fig. 7. Ten cavities appear to be sufficient to attain a steady-state shape; the boundary conditions are different for the initial cavity, but this only affects the first three cavities or fewer. In addition, the final cavity is sometimes a different shape from the previous ones. In these cases, the final cavity shows the shape of an incipient cavity before it has been deformed to its completed shape by the cavity following it. The 4th–9th cavities are representative of the completed shapes that would be created in a large adhesive

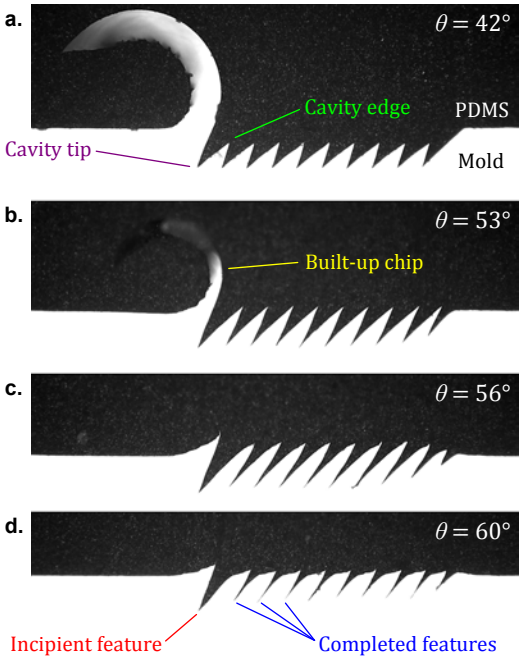

Fig. 7 Micrographs showing the effect of trajectory angle on mold cavity shape. For some trajectories (*a–b*), a continuous chip of built-up material is formed after the final cavity. The chip disappears for $\theta \geq 56°$ (*c–d*).

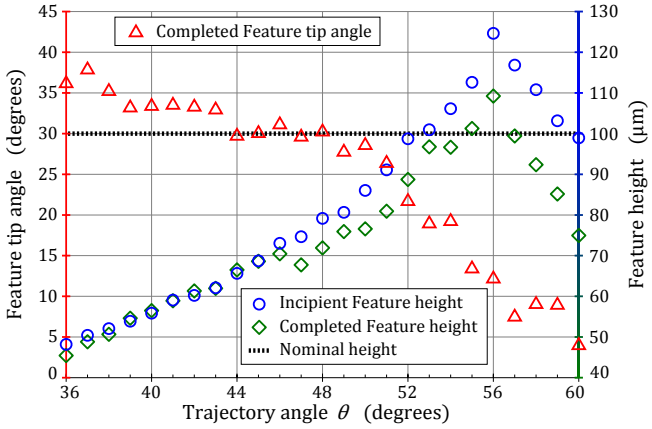

Fig. 8 Geometric data taken from characterization experiment micrographs (Fig. 7). Feature height is measured normal to the mold surface from the tip of the cavity to its upper edge.

array.

The height and angular width of the cavities change with the trajectory angle due to several concurrent effects. For values of θ near 36°, the feature height is significantly less than the nominal height of 100 μm because the cavities intersect one another below the original mold surface (Fig. 7a). As θ increases past 46°, there is an increasingly large difference in height between the incipient feature and the completed features (Fig. 7b), indicating that permanent deformation on the trailing side of the tool is ocurring. The feature height reaches a maximum at $\theta = 56°$, where the trailing-side deformation causes the edges of the cavities to be raised up above the original mold surface (Fig. 7c). As θ is increased further to $\theta = \lambda = 60°$, the features become shorter again and the tip angle diminishes well below the angular width of the blade, indicating that the rearward deformation is causing the cavities to close up at their tips (Fig. 7d). These trends are plotted in Fig. 8.

4.4 Surface Characterization. The surface roughness of adhesive wedges before post-treatment was measured by capturing stereoscopic SEM images and generating 3D topographical plots using the Alicona Imaging MeX software package. Average roughness parameters were computed from 50 μm long line profiles taken across the engaging surfaces of the features. When the micro-machining process was performed using the best lubricant (described in Sec. 3.2.2), the resulting RMS roughness parameter was R_q = 39 nm. This measurement technique can be sensitive to a number of types of calibration and numerical errors, however [44].

Therefore, an independent surface characterization was conducted. Micro-machined PDMS wedges were measured over 2×2 μm and 6×6 μm areas using a Park Systems XE-70 AFM in non-contact mode after excising the wedges and immobilizing them on double-sided tape. The RMS average roughness for a micro-machined wedge before post-treatment was measured as $R_q = 20 \pm 5$ nm for the 2×2 μm scan area and $R_q = 48 \pm 5$ nm for the 6×6 μm scan area. The R_q value was not found to continue to increase with larger scan areas, however. This increasing trend and subsequent limit is a typical result for R_q, and is an indication of the maximum horizontal size scale of the surface roughness [45]. Over these areas, the heights of the tallest asperities were R_p = 61 nm and R_p = 183 nm respectively. This is a very low roughness, comparable to a finely lapped surface [46].

The same measurements were repeated on a micro-machined wedge after post-treatment. For this sample, the RMS roughness parameters were measured as $R_q = 18 \pm 5$ nm for the 2×2 μm scan area and $R_q = 50 \pm 5$ nm for the 6×6 μm scan area. These data do not support the hypothesis that there is a difference in the R_q values before and after post-treatment. Alternatively, the heights of the tallest asperities for this sample were R_p = 45 nm and R_p = 157 nm for the two scan areas. This suggests that the post-treatment process may reduce the surface roughness by limiting the heights of the tallest asperities. This would not significantly affect the value of R_q because the tallest asperities make up a small percentage of the total area.

4.5 Adhesive Tests. Samples of micro-machined adhesives were fabricated to test their adhesive properties. The blade was held at $\lambda = 60°$ and the trajectory was chosen to be $\theta = 48°$, an angle approximately parallel to the rear face of the tool, and found empirically to push most of the displaced material forward. The nominal depth and tip-to-tip spacing were 100 μm and 60 μm, as in Sec. 4.3.

Following the procedure described by Santos *et al.* [47], adhesion force data were collected on an instrumented stage capable of moving the adhesive samples in and out of contact with a flat glass substrate along a specified trajectory and loading the adhesive in both the normal and shear directions. The stage (Velmex MAXY4009W2-S4 and MA2506B-S2.5) is capable of 10 μm positioning resolution in the shear direction and 1 μm in the normal direction. The adhesive samples were mounted on a stationary six-axis force/torque transducer (ATI Gamma SI-32-2.5) with a force measurement resolution of approximately 10 mN. The transducer was mounted on a two-axis goniometer to allow the adhesive and substrate to be precisely aligned. This apparatus is shown in Fig. 9a.

A sample of adhesive is tested by bringing it into contact with the substrate along a 45° approach trajectory until the adhesive reaches a certain preload depth. The preload depth is defined as the distance by which the adhesive is pressed into the substrate, measured normal to the substrate, from the position where the tips of the adhesive

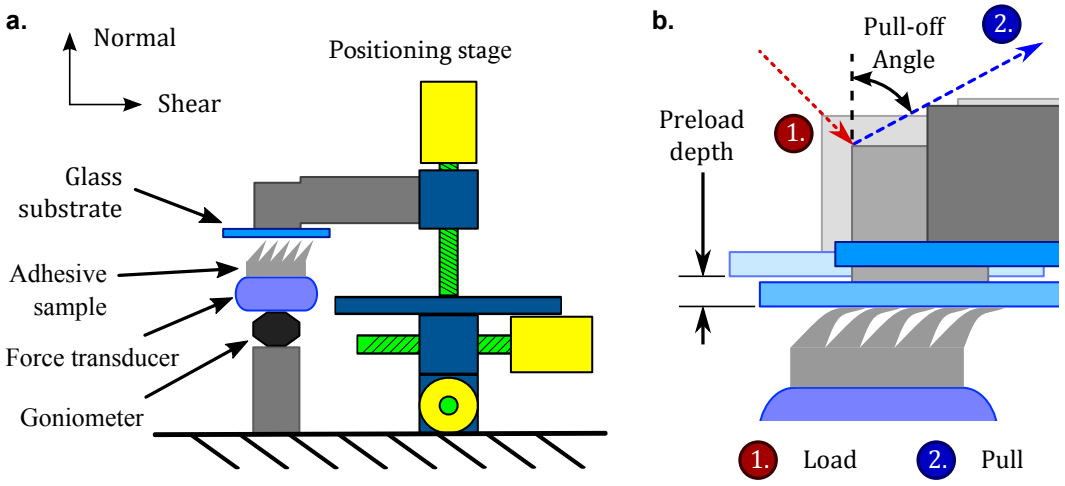

Fig. 9 (*a*) **Diagram of the adhesive testing apparatus, showing the normal and shear directions.** (*b*) **Diagram illustrating the movement of the positioning stage during load-pull tests.**

features make first contact. The preload phase allows for the gradual loading of the features and does not generate slippage. Once the sample is at the appropriate preload depth, it is pulled out of contact along a trajectory at a specified pull-off angle. Such tests are referred to as load-pull tests (see Fig. 9b). To obtain the adhesion limit curve [47], a battery of load-pull tests were performed for preload depths ranging from 30–80 μm and pull-off angles ranging from 0–90°.

Limit curves were generated for a patch of micro-machined adhesive both before and after the post-treatment process step (overall sample area 1.21 cm^2). For comparison, a limit curve was generated for a patch of photolithographic micro-wedge adhesive (overall sample area 0.37 cm^2), consisting of a rectangular pattern of right triangular prisms, approximately 20 μm wide, 80 μm tall, 200 μm long, and with a tip-to-tip spacing of 40 μm between features. These features are pictured in Fig. 1a–b.

For the micro-machined adhesive sample, the normal preload pressure applied at the maximum preload depth of 80 μm was approximately 14.6 kPa before post-treatment and 17.8 kPa after post-treatment. For the photolithographic adhesive sample, the preload pressure at 80 μm was approximately 64 kPa. This indicates that the photolithographic micro-wedges have a higher mechanical stiffness.

The limit curves show the adhesives' performance in force space. Each point corresponds to a combination of normal force and shear force at which failure occurred. The region above the curve is the "safe region": Forces above the curve can be sustained by the adhesive; forces below the curve cause it to fail. The adhesive test results are consistent with the directional adhesion model proposed by Autumn *et al.* for geckos [12], in which adhesion increases with increasing shear force.

As shown in Fig. 10, the photolithographic adhesive produces a maximum adhesive stress of approximately 18 kPa when loaded with a shear stress of approximately 51 kPa, and the micro-machined adhesive with no post-treatment achieves a maximum adhesion of 13 kPa at a shear stress of 37 kPa. After post-treatment, the micro-machined adhesive has a maximum adhesion of 38 kPa at a shear stress of 49 kPa. The measurement uncertainty of these force data is estimated to be 2 kPa in the normal direction and 1 kPa in the shear direction.

At high levels of shear stress, all of the adhesive samples show a "roll-off" in adhesion as increasing numbers of wedges start to slide along the surface.

5 Discussion

The micro-machining process has several advantages over the photolithographic process, including increased yield, greater control over the adhesive feature shape, a wider choice of mold materials, and vastly improved mold turnaround time (a matter of hours instead of weeks). One drawback is that the wax mold may become damaged when the PDMS is extracted from it, and cannot then be used a second time. To make more adhesives, the top layer of the mold is removed and the underlying material is micromachined anew. However, the manufacturing flexibility of micromachined adhesives makes up for this drawback, and they are a particularly attractive option for applications when rapid design iteration is required.

The simple theoretical model introduced in Sec. 2 provides qualitative insight into the mechanics of the micro-machining process and of the effects of varying the tool and approach angles when trying to make closely spaced cavities. However, its force predictions were not substantiated by experimental results. This suggests that a more sophisticated model, for example using large strain finite element modeling, is necessary for accurate predictions.

Empirical evidence shows that a variety of shapes may be created simply by changing the trajectory angle θ, including shapes which do not match the profile of the micro-machining tool (Sec. 4.3). Further experimentation with the blade centerline angle λ and with curved trajectories is also warranted. It is not yet known how different-shaped features would perform in adhesive tests or whether post-treatment would affect these features in the same way. This will be the subject of future research. The data presented here will be valuable in investigating this question by establishing well-defined trends in the geometry of the mold cavities (Fig. 8).

The post-treatment process has a dramatic effect on the micro-machined adhesive's performance: the maximum adhesion increases by nearly a factor of 3. The increase in adhesion may be due to a reduction in the heights of the tallest asperities on the contacting surfaces of the adhesive features (Sec. 4.4). Although these asperities make up a small percentage of the total area of the surface, they have a disproportionate effect on the real area of contact, and hence the generated adhesive force [45].

The post-treated micro-machined wedges also achieve more than twice the maximum adhesion obtained previously with photolithographic wedges. Post-treatment was not found to improve the adhesion of the photolithographic wedges, so the difference in performance is likely due to the difference in geometry. For practi-

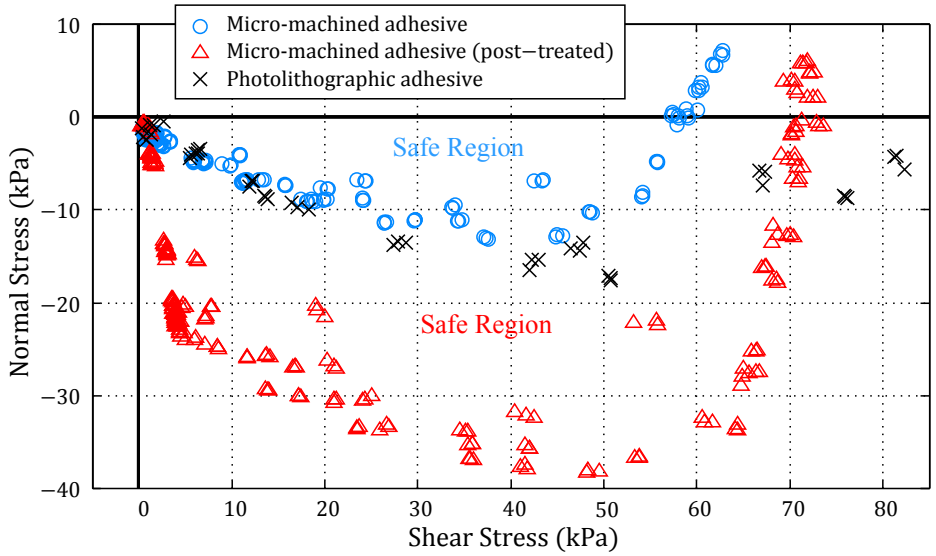

Fig. 10 Comparison of the limit curves for macroscopic arrays of adhesive micro-wedges produced with micro-machined molds and photolithographic molds. The measurement uncertainty of the data is estimated to be 2 kPa in normal and 1 kPa in shear.

cal reasons, it is difficult to make the photolithographic wedges at the same angle of inclination as the micro-machined wedges; instead, they have one vertical and one angled surface. Consequently, they are stiffer in the normal direction and produce a larger elastic force that subtracts from the net adhesive force. This assertion is substantiated by the higher preload pressures required for the photolithographic wedges. In contrast, the micro-machining process affords more freedom to vary the angle of inclination and taper, and the chosen micromachining geometry produces features which are more compliant.

As a further illustration of the effects of varying wedge shape and orientation, the data in Fig. 10 also show much greater adhesion for post-treated micro-machined wedges at low levels of applied shear. As a consequence, the post-treated micro-machined adhesive can support a maximum loading angle of 80° away from the surface for light loads. Whether post-treated or not, the micro-machined adhesives are controllable because they have the property of frictional adhesion [12]: the adhesion increases as the shear load increases, and the adhesion goes to zero as the shear load is removed because the limit curve goes through the origin. This property makes it possible for a climbing robot to detach its feet with very little effort, simply by removing the applied shear force. The result is smooth, efficient climbing.

6 Conclusion and Future Work

In addition to climbing, potential applications for gecko-inspired directional adhesives range from fumble-free football gloves to manufacturing processes involving the handling of materials. However, if these adhesives are to see widespread use outside of the laboratory, a scalable and cost-effective production method must be found.

By following the process discussed in this paper, it is possible to create relatively large patches of gecko-inspired directional adhesives using inexpensive equipment. The micro-wedge micro-machining process also permits greater freedom to control the shapes of the adhesive features than is possible with molds produced by photolithography. In the present case, by creating wedges with two angled surfaces instead of one vertical and one angled surface, and utilizing a simple post-treatment "inking" process, it is possible to obtain a much higher maximum loading angle at low levels of shear loading. This could be useful for applications involving lightweight robots such as micro air vehicles or for handling delicate materials.

The essential requirements of the process described in this paper are (1) a suitable mold material with near-rigid/plastic behavior and (2) the ability to control the trajectory of the tool, thereby controlling the movement of displaced material, so that mold cavities can be spaced close together while simultaneously controlling the cavity shape. The addition of a post-treatment step to the micro-machining process produces more than double the maximum adhesion obtained with corresponding adhesives from photolithographic molds on a flat glass substrate.

Before post-treatment, the micro-machined wedges have an RMS average surface roughness of $R_q = 48 \pm 5$ nm. The post-treatment appears not to affect R_q within the measurement uncertainty, but may reduce the height of the tallest asperities R_p. Additional measurements are required to confirm these results.

The current approach uses inexpensive and readily available materials, including a computer-controlled stage with at least two degrees of freedom (e.g., a CNC milling machine), a microtome blade for the cutting tool, blocks of wax for the molds, and dish soap for the lubricant. Many improvements are clearly possible. The indenting trajectory may be easily modified to create different shaped features, with higher aspect ratios, narrower tips, or different angles. Preliminary experiments suggest that even with the present tool and a suitable lubricant, it may be possible to cut directly into a soft metal. The resulting mold would be much more durable and could survive many molding cycles. Other possibilities include machining a temperature-hardening material such as polymer clay, or using an investment casting process to create a second-generation mold from a more durable material than wax.

The adhesives perform very well on glass, but do not perform as well on rougher surfaces. To improve the adhesion on everyday surfaces with micro-scale roughness, a siping step could be employed after de-molding the adhesive. Specifically, the wedges could be cut perpendicular to their longest dimension at a desired frequency, thereby allowing small, independent sections of the wedge to conform to surface roughness.

Additionally, with suitably precise and stiff positioning equipment, much smaller terminal features should also be possible. As noted in Sec. 1, others have performed nanoscale machining, al-

beit with less control over the tool shape and trajectory. Even more complicated cavity geometries could be generated using a machining apparatus with a rotational degree of freedom (allowing the tool to change its angle during cutting), or by using a custom-shaped micro-machining tool or multiple tools in sequence. Such a process could create a hierarchical structure, with nano-features on the surfaces of larger micro-wedges. Such developments could lead to a gecko-inspired directional adhesive that performs well on rough surfaces, a goal that has thus far remained elusive.

Acknowledgment

The authors thank Rob Dickerson of the Materials Science Lab at the Los Alamos National Laboratory for assistance in characterizing the surface roughness of the features. This work was supported in part by a National Science Foundation NIRT 0708367 and by DARPA DSO. E. V. Eason is supported by a Hertz Foundation Fellowship, an ABB Stanford Graduate Fellowship, and a National Science Foundation Fellowship.

References

[1] Fearing, R., 2012, "Gecko Adhesion Bibliography," http://robotics.eecs.berkeley.edu/~ronf/Gecko/gecko-biblio.html.

[2] Murphy, M. P., and Sitti, M., 2007, "Waalbot: An Agile Small-Scale Wall-Climbing Robot Utilizing Dry Elastomer Adhesives," IEEE/ASME Trans. Mech., **12**(3), pp. 330–338.

[3] Kim, S., Spenko, M., Trujillo, S., Heyneman, B., Santos, D., and Cutkosky, M. R., 2008, "Smooth Vertical Surface Climbing With Directional Adhesion," IEEE Trans. Robot., **24**(1), pp. 65–74.

[4] Daltorio, K. A., Wei, T. E., Horchler, A. D., Southard, L., Wile, G. D., Quinn, R. D., Gorb, S. N., and Ritzmann, R. E., 2009, "Mini-Whegs TM Climbs Steep Surfaces Using Insect-Inspired Attachment Mechanisms," Int. J. Robot. Res., **28**(2), pp. 285–302.

[5] Krahn, J., Liu, Y., Sadeghi, A., and Menon, C., 2011, "A Tailless Timing Belt Climbing Platform Utilizing Dry Adhesives With Mushroom Caps," Smart Mater. Struct., **20**(11), 115021.

[6] Murphy, M. P., Kute, C., Mengüç, Y., and Sitti, M., 2011, "Waalbot II: Adhesion Recovery and Improved Performance of a Climbing Robot Using Fibrillar Adhesives," Int. J. Robot. Res., **30**(1), pp. 118–133.

[7] Hawkes, E. W., Eason, E. V., Asbeck, A. T., and Cutkosky, M. R., 2012, "The Gecko's Toe: Scaling Directional Adhesives for Climbing Applications," IEEE/ASME Trans. Mech., (to appear).

[8] Li, Y., Ahmed, A., Sameoto, D., and Menon, C., 2012, "Abigaille II: Toward the Development of a Spider-Inspired Climbing Robot," Robotica, **30**(01), pp. 79–89.

[9] Northen, M. T., Greiner, C., Arzt, E., and Turner, K. L., 2008, "A Gecko-Inspired Reversible Adhesive," Adv. Mater., **20**(20), pp. 3905–3909.

[10] Jeong, H. E., Kwak, M. K., and Suh, K. Y., 2010, "Stretchable, Adhesion-Tunable Dry Adhesive by Surface Wrinkling," Langmuir, **26**(4), pp. 2223–2226.

[11] Sitti, M., and Fearing, R., 2003, "Synthetic Gecko Foot-Hair Micro/Nano-Structures as Dry Adhesives," J. Adhes. Sci. Technol., **17**(8), pp. 1055–1073.

[12] Autumn, K., Dittmore, A., Santos, D., Spenko, M., and Cutkosky, M., 2006, "Frictional Adhesion: A New Angle on Gecko Attachment," J. Exp. Biol., **209**(18), pp. 3569–3579.

[13] del Campo, A., Greiner, C., and Arzt, E., 2007, "Contact Shape Controls Adhesion of Bioinspired Fibrillar Surfaces," Langmuir, **23**(20), pp. 10235–10243.

[14] Lee, J., Fearing, R. S., and Komvopoulos, K., 2008, "Directional Adhesion of Gecko-Inspired Angled Microfiber Arrays," Appl. Phys. Lett., **93**(19), 191910.

[15] Qu, L., Dai, L., Stone, M., Xia, Z., and Wang, Z. L., 2008, "Carbon Nanotube Arrays With Strong Shear Binding-On and Easy Normal Lifting-Off," Science, **322**(5899), pp. 238–242.

[16] Jeong, H. E., Lee, J.-K., Kim, H. N., Moon, S. H., and Suh, K. Y., 2009, "A Nontransferring Dry Adhesive With Hierarchical Polymer Nanohairs," Proc. Natl. Acad. Sci. USA, **106**(14), pp. 5639–5644.

[17] Murphy, M. P., Aksak, B., and Sitti, M., 2009, "Gecko-Inspired Directional and Controllable Adhesion," Small, **5**(2), pp. 170–175.

[18] Parness, A., Soto, D., Esparza, N., Gravish, N., Wilkinson, M., Autumn, K., and Cutkosky, M., 2009, "A Microfabricated Wedge-Shaped Adhesive Array Displaying Gecko-Like Dynamic Adhesion, Directionality and Long Lifetime," J. R. Soc. Interface, **6**(41), pp. 1223–1232.

[19] Sameoto, D., and Menon, C., 2009, "Direct Molding of Dry Adhesives With Anisotropic Peel Strength Using an Offset Lift-Off Photoresist Mold," J. Micromech. Microeng., **19**(11), 115026.

[20] Kwak, M. K., Jeong, H.-E., Kim, T.-i., Yoon, H., and Suh, K. Y., 2010, "Bio-Inspired Slanted Polymer Nanohairs for Anisotropic Wetting and Directional Dry Adhesion," Soft Matter, **6**(9), pp. 1849–1857.

[21] Sameoto, D., and Menon, C., 2010, "Recent Advances in the Fabrication and Adhesion Testing of Biomimetic Dry Adhesives," Smart Mater. Struct., **19**(10), 103001.

[22] Gillies, A. G., and Fearing, R. S., 2011, "Shear Adhesion Strength of Thermoplastic Gecko-Inspired Synthetic Adhesive Exceeds Material Limits," Langmuir, **27**(18), pp. 11278–11281.

[23] Yu, J., Chary, S., Das, S., Tamelier, J., Pesika, N. S., Turner, K. L., and Israelachvili, J. N., 2011, "Gecko-Inspired Dry Adhesive for Robotic Applications," Adv. Funct. Mater., **21**(16), pp. 3010–3018.

[24] Jin, K., Tian, Y., Erickson, J. S., Puthoff, J., Autumn, K., and Pesika, N. S., 2012, "Design and Fabrication of Gecko-Inspired Adhesives," Langmuir, (to appear).

[25] Hawkes, E. W., Ulmen, J., Esparza, N., and Cutkosky, M. R., 2011, "Scaling Walls: Applying Dry Adhesives to the Real World," *Proceedings IEEE/RSJ International Conference on Intelligent Robots and Systems*, pp. 5100–5106.

[26] Soto, D., Hill, G., Parness, A., Esparza, N., Cutkosky, M., and Kenny, T., 2010, "Effect of Fibril Shape on Adhesive Properties," Appl. Phys. Lett., **97**(5), 053701.

[27] Gong, J., Lipomi, D. J., Deng, J., Nie, Z., Chen, X., Randall, N. X., Nair, R., and Whitesides, G. M., 2010, "Micro- and Nanopatterning of Inorganic and Polymeric Substrates by Indentation Lithography," Nano Lett., pp. 2702–2708.

[28] Autumn, K., Sitti, M., Liang, Y. A., Peattie, A. M., Hansen, W. R., Sponberg, S., Kenny, T. W., Fearing, R., Israelachvili, J. N., and Full, R. J., 2002, "Evidence for van der Waals Adhesion in Gecko Setae," Proc. Natl. Acad. Sci. USA, **99**(19), pp. 12252–12256.

[29] Hill, R., Lee, E. H., and Tupper, S. J., 1947, "The Theory of Wedge Indentation of Ductile Materials," Proc. R. Soc. A, **188**(1013), pp. 273–289.

[30] Hill, R., 1950, *The Mathematical Theory of Plasticity*, 1st ed., Clarendon Press, Oxford.

[31] Ernst, H., and Merchant, M. E., 1941, "Chip Formation, Friction and High Quality Machined Surfaces," *Surface Treatment of Metals*, American Society for Metals, Cleveland, OH, pp. 299–378.

[32] Merchant, M. E., 1945, "Mechanics of the Metal Cutting Process. I. Orthogonal Cutting and a Type 2 Chip," J. Appl. Phys., **16**(5), pp. 267–275.

[33] Merchant, M. E., 1945, "Mechanics of the Metal Cutting Process. II. Plasticity Conditions in Orthogonal Cutting," J. Appl. Phys., **16**(6), pp. 318–324.

[34] Johnson, W., Sowerby, R., and Venter, R. D., 1982, *Plane-Strain Slip-Line Fields for Metal-Deformation Processes*, Pergamon Press, Oxford.

[35] Bodsworth, C., Halling, J., and Barton, J. W., 1957, "The Use of Paraffin Wax as a Model Material to Simulate the Plastic Deformation of Metals," J. Iron Steel Inst., **185**, pp. 375–383.

[36] Bitans, K., and Brown, R. H., 1965, "An Investigation of the Deformation in Orthogonal Cutting," Int. J. Mach. Tool Des. Res., **5**(3), pp. 155–165.

[37] Meguid, S. A., and Collins, I. F., 1977, "On the Mechanics of the Oblique Cutting of Metal Strips With Knife-Edged Tools," Int. J. Mech. Sci., **19**(6), pp. 361–371.

[38] Hill, R., and Lee, E. H., 1946, "The Theory of Wedge Penetration at Oblique Incidence and its Application to the Calculation of Forces on a Yawed Shot Impacting on Armour Plate at Any Angle," Theoretical Research Report 1/46, UK Ministry of Supply Armament Research Department.

[39] Li, X., Yu, H., Xu, J., Liu, A., and Lv, H., 2009, "Model of Micro-Cutting and Analysis of Micro Cutting Force," *Proceedings IEEE International Conference on Mechatronics and Automation*, pp. 1541–1545.

[40] Johnson, W., and Mellor, P. B., 1973, *Engineering Plasticity*, Van Nostrand Reinhold Co., London.

[41] Childs, T. H. C., and Rowe, G. W., 1973, "Physics in Metal Cutting," Rep. Prog. Phys., **36**(3), pp. 223–288.

[42] Molinari, A., and Moufki, A., 2008, "The Merchant's Model of Orthogonal Cutting Revisited: A New Insight Into the Modeling of Chip Formation," Int. J. Mech. Sci., **50**(2), pp. 124–131.

[43] Hirst, W., and Howse, M. G. J. W., 1969, "The Indentation of Materials by Wedges," Proc. R. Soc. A, **311**(1506), pp. 429–444.

[44] Marinello, F., Bariani, P., Savio, E., Horsewell, A., and De Chiffre, L., 2008, "Critical Factors in SEM 3D Stereo Microscopy," Meas. Sci. Technol., **19**(6), 065705.

[45] Bhushan, B., 1999, *Principles and Applications of Tribology*, Wiley, New York.

[46] Bhushan, B., ed., 2010, *Springer Handbook of Nanotechnology*, 3rd ed., Springer, Berlin.

[47] Santos, D., Spenko, M., Parness, A., Kim, S., and Cutkosky, M., 2007, "Directional Adhesion for Climbing: Theoretical and Practical Considerations," J. Adhes. Sci. Technol., **21**(12–13), pp. 1317–1341.